Nonlocal Measurement as a Probe of the Spin Hall Effect in Topological Insulators

Gregory M. Stephen, Owen A. Vail, Jennifer E. DeMell, Aubrey T. Hanbicki, Patrick J. Taylor, and Adam L. Friedman

Phys. Rev. Applied **16**, 034007 — Published 3 September 2021

DOI: 10.1103/PhysRevApplied.16.034007

Nonlocal measurement as a probe of the spin Hall effect in topological insulators

Gregory M. Stephen[1*], Owen. A Vail[2], Jennifer E. DeMell[1], Aubrey T. Hanbicki[1], Patrick J. Taylor[2], Adam L. Friedman[1*]

[1]*Laboratory for Physical Sciences, 8050 Greenmead Dr., College Park, MD 20740*
[2]*Army Research Laboratory, 2800 Powder Mill Rd., Adelphi, MD 20783*

*Corresponding authors. Email: gstephen@lps.umd.edu, afriedman@lps.umd.edu

Abstract

Topological insulators (TIs) are promising candidates for novel computing device designs. In particular they have great potential for spintronic devices where utilization of electron spin rather than charge would allow for lower power and higher performance computing in next generation architectures. Efficient conversion between spin and charge signals is crucial to spintronic technology. TIs provide highly efficient spin-to-charge conversion as a result of their unique topological properties. One way to electrically quantify conversion efficiency is with the spin Hall effect (SHE). Here we present SHE measurements of the topological insulator $Bi_2Te_{2.5}Se_{0.5}$. Because of the topological nature of this material, we can measure the SHE without the use of ferromagnetic injectors or detectors. Using the non-local resistance, we measure spin Hall angles up to 2.4 with spin lifetimes up to 9 ps. Furthermore, the ferromagnet-free measurement allows for quick diagnostics of the spin properties without the need to fabricate multilevel devices.

Keywords: Bismuth Selenide, Bismuth Telluride, topological insulator, inverse spin Hall effect

Introduction

Spintronic devices manipulate the electron spin for storage and processing of information, allowing for orders of magnitude reduction of power consumption and increased performance compared to the solely charge-based electronics. [1] Spin-based devices such as spin transfer torque (STT) and spin orbit torque (SOT) magnetic random access memory (MRAM) are increasingly commonplace in high performance computing strategies. For such devices to reach their maximum potential requires efficient spin-to-charge conversion, long spin coherence lengths, and long spin relaxation times. Materials currently used in these devices such as β-W, Pt, or Ta do not possess high enough spin-to-charge conversion rates for spintronic devices to compete with CMOS. [2–4] However, topological materials, particularly topological insulators (TIs), can have spin metrics high enough to enable competitive spintronic devices. [5,6]

In TIs, band inversion gives rise to topologically protected surface states with linear energy dispersions (Dirac cones) resulting in Dirac fermions possessing high mobilities and Fermi velocities. The band inversion also fixes the fermion spin orthogonal to its momentum, resulting in highly efficient spin-to-charge conversion. The spin Hall angle, $\theta_{SH} = I_s/I_e$, a measure of the spin-to-charge conversion efficiency expressed as the ratio of spin to charge current, can far exceed unity in TIs, with values reported as high as 425 for $(Bi_{0.5}Sb_{0.5})_2Te_3$. [7] In general, measurements of TI spintronic properties have been restricted to local measurements which do not accurately reflect the macroscopic effects of the entire TI film. Due to various contributing factors, including surface roughness, polycrystallinity, and defect doping, the local behavior of topological insulators can be vastly different from the macroscopic properties utilized in devices. [8]

The macroscopic spin-to-charge transfer efficiency can be extracted from measuring such phenomena as the Rashba-Edelstein effect (REE), [9] a surface effect that results in spin accumulation, and the spin Hall effect (SHE), a bulk effect which produces a spin polarized current. [10] While REE measurements can be complicated by the need for effective tunnel barriers, [11–13] the SHE is more straightforward. In the SHE, a flowing charge current in a macroscopic channel produces an orthogonal spin current either through extrinsic scattering [10] or intrinsic spin-orbit interactions [14]. The SHE can be observed optically using Kerr microscopy [15], though this cannot be incorporated into imbedded electronic devices. Direct electrical measurements are possible but can be difficult to distinguish, especially in material with low spin Hall angles. The SHE can be enhanced by spin injection, either by spin-pumping from a ferromagnetic insulator [2] or by direct injection of a spin-polarized current from a metallic ferromagnet. [15] While useful for extracting the spin Hall characteristics of heavy metals, metallic ferromagnets can interfere with the topological states at the interface. [16–18]

As theoretically demonstrated by Abanin, *et al.*, [19], the SHE can also be measured in a Hall bar geometry without ferromagnetic contacts by utilizing a combination of the SHE and inverse spin Hall effect (ISHE). The high spin Hall angles and long diffusion lengths found in TIs make them ideal for this technique as contacts can be spaced far apart, simplifying the lithographic process. [20] In this study, we show this SHE/ISHE method can readily be used to measure the spintronic properties of TI films. We focus on $Bi_2Te_{2.5}Se_{0.5}$ because our previous work demonstrated that this alloy, with its slightly Te-rich composition, exhibits a somewhat improved surface state conduction compared to Bi_2Te_2Se or Bi_2Se_3. [21] We measure the spin Hall effect without ferromagnetic injector or detector contacts and extract spin Hall angles of order 1, spin relaxation times in the 1-10 ps timescale and spin diffusion lengths around 1 μm. All of these values are commensurate with literature values for other TIs. While the end precision of the fit results using this technique are limited relative to direct first order observation techniques, the power of this methodology comes from the simplicity of the device design, opening the possibility for use as a diagnostic measurement in complex devices.

Results/Discussion

50 nm thick epitaxial films of $Bi_2Te_{2.5}Se_{0.5}$ were grown *via* molecular beam epitaxy on semi-insulating GaAs(001) substrates at a substrate temperature of 290°C. X-ray diffraction, RHEED and TEM confirm high quality epitaxy with a sharp substrate interface, as described elsewhere. [21] The $Bi_2Te_{2.5}Se_{0.5}$ films were patterned into multiprong Hall bars with contact spacings from 0.5 µm to 5.75 µm. The mesas were defined by electron beam lithography with 200 nm poly(methyl methacrylate) (PMMA) resist and etched with an Ar plasma. An optical image of the device is shown in **Figure 1(a)**. Samples were measured in a closed-loop He cryostat set within the poles of a 1 T resistive electromagnet. Electrical measurements were performed using DC bias and averaged over many measurements in order to improve the signal-to-noise ratio. Unless otherwise noted, all measurements were carried out at 3 K.

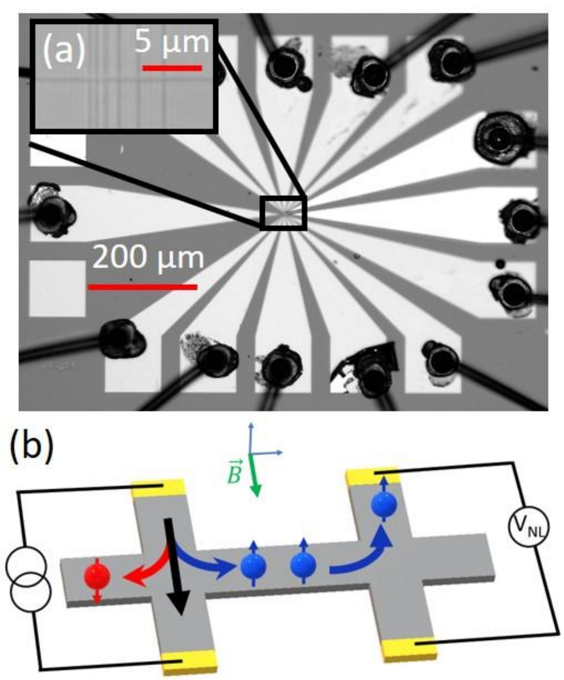

Figure 1: Device design. (a) Optical image (inset image taken with a confocal laser microscope) of the $Bi_2Te_{2.5}Se_{0.5}$ Hall bar. The avenue and contact arms are 0.25 μm wide and patterned by electron beam lithography. Spacings between adjacent contacts from 0.5 μm up to 2 μm (b) Schematic showing the geometry of the spin Hall measurement. A local charge current between the left two contacts produces a pure spin current in the channel through the spin Hall effects. This spin current then produces a non-local voltage at the right set of contacts *via* the inverse spin Hall effect. A magnetic field is applied along the charge current direction.

The schematic drawing in **Figure 1(b)** demonstrates the electrical configuration of the measurement. When a charge current passes between one pair of transverse contacts (left), a spin current is generated along the central Hall bar channel due to the spin Hall effect. The pure spin current then produces a measurable non-local voltage, V_{NL}, due to the inverse spin Hall effect at a second set of transverse contacts (right) located outside of the current path. [19] The spin current can be further manipulated by applying an external magnetic field and monitoring the field dependence of the non-local spin Hall resistance, R_{NL}^{SH}, at the non-local contacts. As indicated in **Figure 1(b)**, the magnetic field is applied parallel to the applied current. With this applied field, the spins begin to precess at the Larmor frequency. Sweeping the magnitude of the magnetic field causes precessional dephasing, also known as the Hanle effect, resulting in a pseudo-Lorentzian R_{NL}^{SH} *vs.* magnetic field. This technique was demonstrated in a variety of materials including graphene and Cd_3As_2 [20,22,23].

A conventional Hanle measurement requires fabrication of a spin-valve, which brings unique challenges to measuring topological materials. [24] In addition to reflection effects from the tunnel barriers limiting the spin parameters beyond anything within the TI, this measurement requires an out-of-plane magnetic field which, in itself, can destroy the topological states. Additionally, if the spin relaxation time is long enough, the Hanle curve could be wider than the anisotropy field of the ferromagnets, rotating the ferromagnetic moments out of plane and nullifying the conditions for precession independent of the spin scattering mechanism or topological state.

Parameters such as spin Hall angle, θ_{SH}, spin diffusion length, λ_s, and spin relaxation time, τ_s, are extracted from the magnetic field dependence of the induced voltage, described by: [19]

$$R_{NL}^{SH}(B) = \frac{1}{2}\theta_{SH}^2\rho\frac{W}{\lambda_s}Re\left[\sqrt{1+iB\Gamma\tau_s}e^{-\frac{L}{\lambda_s}\sqrt{1+i\tau_s\Gamma B}}\right] \quad (1).$$

In this equation, W and L are the width and length of the spin-current channel and ρ is the channel resistivity, which can be measured independently. Other parameters in Eq. (1) include the gyromagnetic ratio $\Gamma = g\mu^*/\hbar$, where g is the Landé g-factor and $\mu^* = \frac{e\hbar}{2m^*}$ is the effective magnetic moment of the electron. Because τ_s and Γ are coupled within the model, knowledge of g is essential for an accurate measurement of the spin relaxation time. Provided the g-factor is independent of temperature and applied current, relative changes in the response due to variation of these experimental parameters can be attributed to τ_s. Additionally, the uncertainty of the spin Hall angle is compounded by errors in both ρ and the fitting of λ_s. While these considerations limit the end precision of the fit results relative to direct first order observation techniques, the power of this methodology comes from the simplicity of the device design, enabling its use as a diagnostic measurement in complex devices. For example, a simple Hall bar could be fabricated alongside a more complicated device structure. Measuring how the spin Hall signal, or even just the amplitude of the non-local voltage, changes over time could be used to track degradation of the TI layer. Any geometrical artifacts would be constant within the device and the decrease in amplitude of the non-local voltage would directly track the degradation of the spin properties.

A characteristic R_{NL}(B) sweep (black squares) and the associated fit (red line) for a spacing of L = 1.75 μm and current I = +50 μA is shown is **Figure 2(a)**. A 2nd order polynomial background was subtracted to account for local Hall and classical magnetoresistance effects. The background subtraction is discussed further in the **Supplementary Materials**.[39] The Hall bars utilized in this experiment were designed to allow for length dependence measurements to be conducted within a single device, even after accounting for variations in contact quality from lithography and sample wire. The basic measurement shown in **Figure 2(a)** was repeated at a variety of bias currents and contact spacings. Bias dependence is shown in **Figure 2(b)** with length dependence in **Figure 2(c)**. Both of these plots were constructed by plotting the amplitude of the non-local resistance measured at B=0 T after subtracting the background. The non-local signal has a peak at low bias currents with a noticeable saturation at higher applied currents. A similar saturation of spin current at higher applied charge currents was observed in Bi_2Te_2Se and graphene and was attributed to a reduced polarization efficiency at higher currents. [25,26] There is a modest increase in the length dependence of the data (**Figure 2(c)**) between L = 0.75 µm to 1.25 µm. We attribute the increased resistance at this length to a decrease in remnant local effects which obscure the non-local signal. The local signal decreases much faster than the exponential decay of the spin signal. So, by 2.5 µm, the remaining non-local change is almost entirely from the spin current.

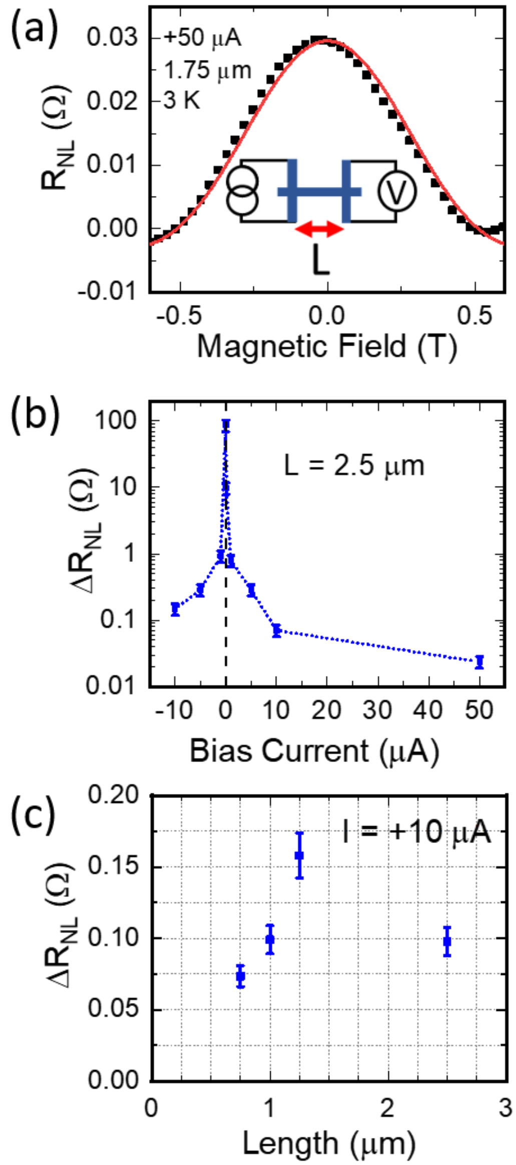

Figure 2: Non-local spin signal (a) Characteristic $R_{NL}(B)$ for I = +50 μA and Δx = 1.75 μm (points)with the associated fit (line) to Eq 1. (b) The non-local resistance R_{NL} versus bias current peaks at low current due to increased spin polarization at low currents. (c) amplitude ΔR_{NL} of the non-local signal versus contact spacing at a fixed current of 10 μA. The signal strengthens up to 1.25 μm, likely due to a reduction in residual local background, and decreases at 2.5 μm.

The spacing dependencies of spin parameters (θ_{SH}, λ_s, and τ_s) at a constant bias current of I = +10 μA are given in **Figure 3(a-c)**, with the bias dependence at a fixed length of L = 2.5 μm in **Figure 3 (d-e)**. Again, we expect the spin signal at this distance to be mostly a spin current.

Error bars are determined from the uncertainty in fitting to Eq. 1. The bias dependence of all three parameters is similar and reflects the overall non-local resistance change (**Figure 2(b)**). A maximum spin Hall angle (**Figure 3(d)**) of $\theta_{SH} = 2.4$ is measured at $I = +10$ nA. This is comparable to other TIs and an order of magnitude larger than what is found in heavy metals. [23] Literature values for the spin Hall angles in $Bi_2Te_xSe_{3-x}$ are summarized nicely by Farzaneh, *et al.* [33] and range from 0.08 for Bi_2Te_3 up to 3.5 for Bi_2Se_3. [27] While the highest spin Hall angles are measured *via* spin torque ferromagnetic resonance (FMR), $\theta_{SH} = 0.16$ for Bi_2Se_3 is the highest electrically sourced and detected spin Hall angle. [28] Our maximum measured spin Hall angle is more than 10x higher than this, and comparable to FMR results, [29,30] which suggests the 5:1 Te:Se ratio used here significantly improves the spin-charge conversion efficiency over pure Bi_2Te_3 and comes close to the maximum measured value for Bi_2Se_3.

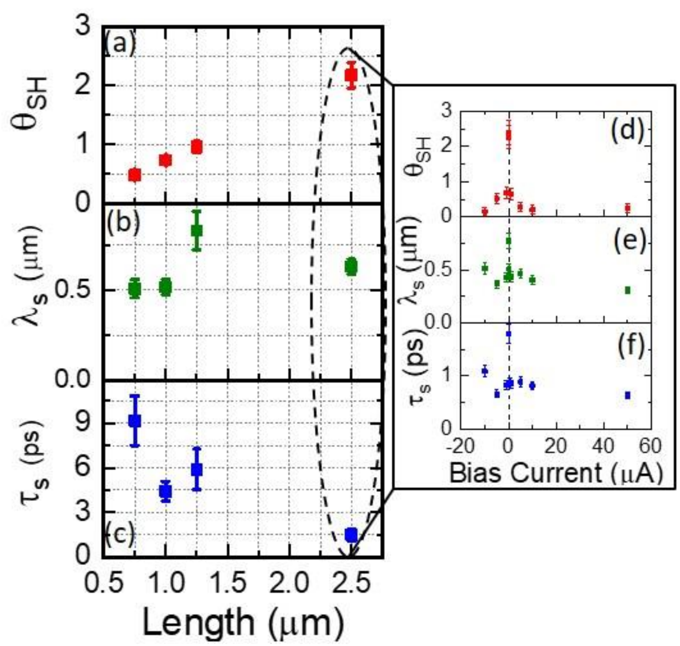

Figure 3: Spin parameter length and bias dependencies. The (a) spin Hall angle, (b) spin diffusion length, and (c) spin lifetime as functions of contact spacing. The respective bias dependencies are given in the insets. The spin Hall angle θ_{SH}, increases linearly with spacing. While the low current

increase tracks ΔR_{NL}, the increase between 1.25 µm and 2.5 µm can be attributed to a near-complete removal of lingering local backgrounds. (b) the spin diffusion length λ_s is relatively constant with an anomalous peak at 1.25 µm, while (c)the spin relaxation time τ_s decreases steadily with increasing contact spacing. (d-f) All three parameters follow similar bias dependencies as ΔR_{NL} shown in 3b, as a result of the saturation of the spin signal and decreased spin to charge conversion efficiency at higher bias currents.

The results presented here are comparable to reported FMR results with the convenience, simplicity, and accessibility of an all-electrical measurement. One drawback of this method is the tendency towards large fitting errors in θ_{SH}. The spin Hall angle only appears in Eq. (1) as part of the amplitude coefficient, $\theta_{SH}^2 \rho W / 2\lambda_s$. Because fitting can only uniquely determine a single overall amplitude, the uncertainty in θ_{SH} becomes dependent on precise knowledge of the other parameters. This is compounded by the spin diffusion length, λ_s, being another fitting parameter within the amplitude coefficient. However, because λ_s also occurs in the exponent of Eq. (1), it is somewhat decoupled from θ_{SH}.

The spin diffusion length (**Figure 3(b,e)**) has a maximum value of λ_s = 0.78 µm, which is of the same order of magnitude as conductive metals such as Au(0.06 to 0.17 µm) and Cu(0.2 to 1 µm). [31] While the spin diffusion length for the surface states of a TI is expected to be long due to spin momentum locking, the bulk spin diffusion length should be shorter due to increased spin scattering from the large spin orbit coupling and momentum scattering caused by grain boundaries. [32] Because our samples have predominantly bulk conduction, the spin diffusion length, and the spin parameters in general, are characteristic of the spin-orbit coupled bulk states.

Figures 3(c) and **3(f)** show the spin lifetime, τ_s. As the spin lifetime is coupled to the gyromagnetic ratio in the model, the accuracy of this parameter can vary significantly depending on the material system. Again, the gyromagnetic ratio is given by $\Gamma = \frac{eg}{2m^*}$, where g is the Landé g-factor and m^* is the effective mass. Both parameters are non-trivial to measure and can vary within a material system. Without a precise measurement for a specific sample, the extracted value of τ_s should be taken as a rough estimate. A particularly egregious example is Cd_3As_2 where literature values for g range from 2 to 100. [33]. We assume values of g = 23 and m^* = 0.25 m_0 based on a review of the literature on the $Bi_2Te_xSe_{3-x}$ system. [34–36] As g and m^* are multiplicative factors of τ_s, the relative changes with respect to bias, temperature and spacing are reliable regardless of the accuracy of g and m^*, only the absolute magnitude of τ_s changes. Thus, for a single sample or device, this method can effectively track changes in the spin parameters as functions of processing steps, time or other extrinsic parameters. Therefore, this method is a way to efficiently screen topological materials without the many levels of fabrication needed for conventional spin devices, although absolute precision can be a limitation.

The length dependence observed in **Figure 3 (a-c)** requires further consideration. One would expect λ_s, τ_s and θ_{SH} to be largely independent of contact spacing as they are intrinsic properties of the material. We observe the spin Hall angle θ_{SH} (**Figure 3(a)**) increases linearly with contact spacing, from 0.48 ± 0.05 at Δx = 0.75 μm to 2.2 ± 0.2 at Δx = 2.5 μm. This can be partially attributed to a background signal which decreases over this range, leading to a more significant contribution of the SHE in the overall signal, resulting in a larger measured θ_{SH}. An increasing spin signal with contact spacing, as observed in spin pumping experiments on permalloy/Pt thin films [37] would further magnify this effect. The spin diffusion length (**Figure 3(b)**) has a similar length dependence as R_{NL} (**Figure 2(c)**). With an average of λ_s = 0.6 ± 0.1 μm, the spin diffusion length is relatively unchanged as a function of contact spacing aside from a peak λ_s = 0.8 μm at L = 1.25 μm. The spin lifetime (**Figure 3(c)**) decreases by almost an order of magnitude from 9.2 ps at 0.75 μm to 1.5 ps at 2.5 μm. These spin lifetimes are comparable to values found in Si, but considerably less than what would be expected for surface states of a topological insulator. [38]

This is likely a result of the high doping concentration. As the transport is dominated by the bulk states, the spin relaxation is reduced by the high spin-orbit coupling within the material. The parameters extracted from this model constitute lower bounds on the sample's intrinsic properties. The model proposed by Abanin, *et al*. assumes a narrow channel width $W << \lambda_s$ so the SHE contribution overwhelms the Ohmic contribution which decays as $e^{-\pi|x|/W}$. As the channel width approaches λ_s, the relative contribution of the spin Hall effect decreases, providing reduced parameters.

The observed non-local voltage could be caused by several effects aside from the SHE, including Ohmic leakage (bypass effect), weak antilocalization (WAL), or quasiballistic scattering from the current path to the non-local voltage contacts. These effects contribute to the background, but can be systematically eliminated as causes of the pseudo-Lorentzian peak in R_{NL}(B). The simplest to exclude is WAL, which can have a peak-like magnetic field dependence similar to the SHE. As WAL is a local effect, it must be accompanied by a comparable Ohmic contribution. Therefore, if WAL, or even local Hall effects are affecting the SHE measurement, the measured non-local behavior should be similar to the local signal. The field dependence of the local resistance, R_{xx}, is shown in **Figure 4(a)**, with the measurement geometry in the inset. More comprehensive WAL data for these films is found elsewhere, and show a phase coherence length of 200 nm. [21] There is a WAL contribution to the pseudo-linear behavior for low fields, but it is too weak relative to the background MR to explain the prominent peak in the non-local signal. Additionally, the sign of the WAL contribution is the opposite sign compared to our observations of R_{NL}. Finally, WAL in topological materials depends on the spin-orbit coupling and local resistance, both of which are independent of the current. The SHE signal changes significantly with current, as seen in **Figure 2(a)** and **3(d-f)**, further excluding WAL.

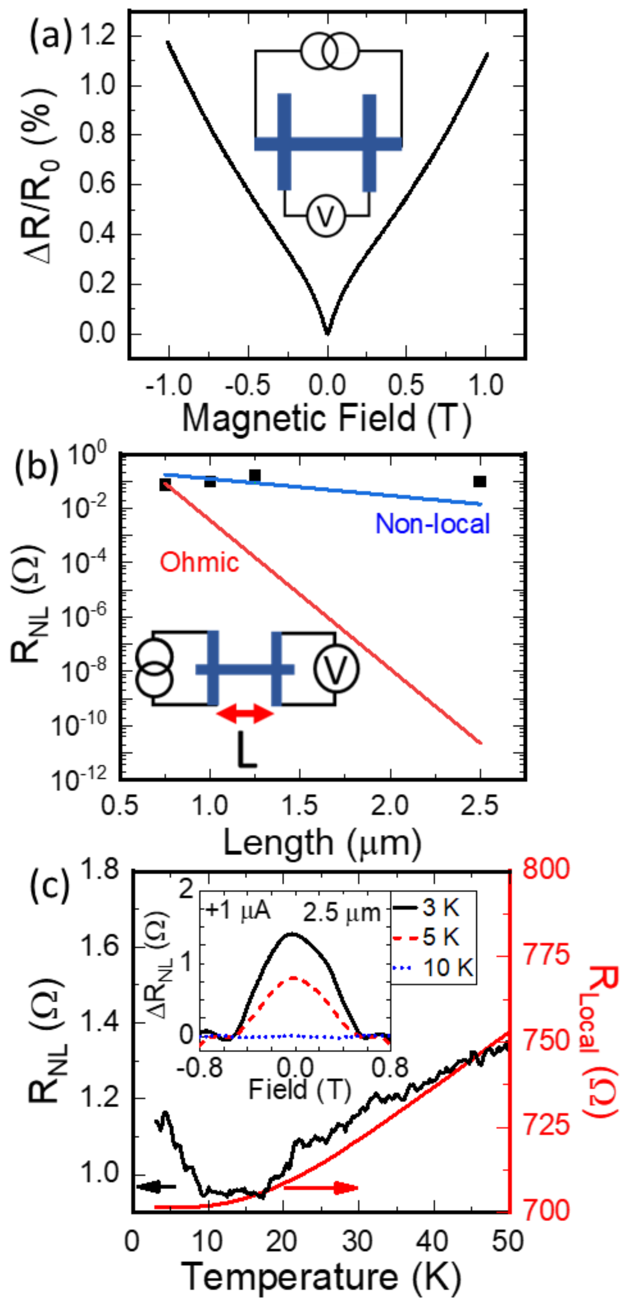

Figure 4: Local Resistance Effects (a) Local magnetoresistance of $Bi_2Te_{2.5}Se_{0.5}$ thin film. The WAL cusp is weakly visible over the background linear MR. Similar behavior is not present in Figure 2(a), ruling out WAL as a contributing factor. (b) Measured non-local signal (black squares) along with the expected non-local (blue) and local(red) contributions. The expected non-local contribution is calculated using the average values of τ_s, λ_s and θ_{SH} from the data in Figure 3. The Ohmic contribution decreases much faster that what is measured, which more closely follows the expected non-local behavior (c) Temperature dependence of the non-local resistance (black) and the local resistance (red). The low temperature decrease in R_{NL} disappears at 10 K when the signal

in the field dependent data (inset) vanishes. Additional temperature data up to 20 K is given in the Supplemental Materials and demonstrates the signal has disappeared completely.

An Ohmic contribution can be excluded by considering the length and temperature dependence of the non-local signal. For a rectangular sample, the Ohmic resistance is given by

$$R_{\mathrm{Ohmic}} = \frac{\rho}{\pi} \ln \frac{\cosh(\pi L/W)+1}{\cosh(\pi L/W)-1} \ (2),$$

where again ρ is the resistivity, W is the width of the Hall bar, and L is the spacing between the source and measurement contacts. In the case of our Hall bars, $L >> W$ so this contribution approaches zero, especially as the contact spacing increases. In contrast, from Eq. (1) the expected length dependence of the non-local resistance at zero magnetic field is given by

$$R_{NL} = \frac{1}{2} \theta_{SH}^2 \rho \frac{W}{\lambda_s} e^{-L/\lambda_s} \ (3).$$

The non-local resistance should also approach zero for $L >> W$, but much slower than an Ohmic contribution. **Figure 4(b)** shows the length dependence of the measured non-local resistance (points) and the expected behavior of a non-local (blue line) and Ohmic (red line) contribution, as dictated by Eq. (2) and (3), respectively. The expected values are calculated using the average values for θ_{SH} and λ_{s}, found from fitting to Eq. (1), as discussed below and the Ohmic contribution incorporates the measured resistivity of 800 μΩ-cm. The measured non-local resistance has a length dependence described well by Eq. (3).

A further disqualifying consideration for an Ohmic contribution is the temperature dependence. Because an Ohmic contribution is governed by the geometry of the sample, it should not vary with temperature beyond the monotonic temperature dependence of the longitudinal resistivity. **Figure 4(c)** shows the measured local resistance (red line, right axis) at B = 0 T with no background subtracted as temperature is swept from 3 K to 30 K in a sample with L=2.5 μm and the expected monotonic increase with temperature. The measured R_{NL} (black line, left axis) measured under the same conditions has a distinct temperature dependence. In these data, there is a distinct decrease in the non-local resistance between 3 K and 10 K, before it plateaus and begins to increase linearly at a similar rate as the local resistance. This corresponds to the reduction of the non-local resistance signal with temperature seen in the inset of **Figure 4(c)**. The contribution of R_{NL}, apparent in the low temperature portion of the data, disappears at 10 K. At higher temperature, R_{NL} increases monotonically like the local resistance. While this remaining background is therefore composed of an Ohmic terms, it is the positive spin Hall component that induces the oscillatory signal in $R_{NL}(B)$.

The observed temperature dependence also rules out the quasiballistic effect, which should be negative at low temperatures and cross over to a positive value at some finite temperature. [22] The temperature-dependent component of R_{NL} seen in **Figure 4(c)** is of the same sign as the local resistance and never passes through zero, that is a negative R_{NL} for a positive applied current, indicating that the quasiballistic effect is not a significant factor. It should be noted that the quasiballistic effect also requires the thickness of the sample to be larger than the mean free path of the charge carriers. If the film is thinner than the mean free path, carriers scatter off the film boundaries before reaching the non-local contacts, minimizing the quasiballistic contribution. In the $Bi_2Te_{2.5}Se_{0.5}$ system measured here, the mean free path is on the order of 4-14 nm, thinner than the 50 nm sample thickness. In samples with sufficiently high mobility, the quasiballistic effect can be disregarded on the mean free path alone.

While the spin signal is still dominant over background effects as described with **Figure 4** and the relevant discussion, the local background still obscures the full spin signal. To get measured values close to the actual intrinsic parameters of the sample, the spin signal must not only be large enough to dominate local background effects, the spacing must be long enough for the local effects to be nearly non-existent. This is evidenced by the initial increase in R_{NL} *vs.* length seen in **Figure 2(c)**. However, these artifacts are entirely geometry dependent. Therefore, the technique would be considerably more useful in comparing the change between devices of identical geometry, or a single device over time. The absolute values of θ_{SH}, λ_s, and τ_s may be inaccurate compared to the actual intrinsic values, but the relative change will be unaffected as ρ, g, and m^* become irrelevant scaling factors when looking at the relative change.

Conclusion

We electrically investigated the spin Hall effect in $Bi_2Te_{2.5}Se_{0.5}$ without the use of ferromagnetic injectors or detectors. Our results compare favorably to literature results for Bi_2Se_3 and Bi_2Te_3. $Bi_2Te_{2.5}Se_{0.5}$ has improved spin Hall angle compared to Bi_2Te_3 and comparable to Bi_2Se_3. The non-local, ferromagnet-free measurement technique used here yielded similar spin figures of merit as exist in literature, where more complicated device structures were used, demonstrating the utility of this measurement geometry. With the non-local measurement technique constituting a lower bound on the spin Hall angle, our results suggest $Bi_2Te_{2.5}Se_{0.5}$ is a promising candidate for further investigation for spintronic applications.

Acknowledgements:

The authors gratefully acknowledge critical assistance from LPS support staff including G. Latini, J. Wood, R. Brun, P. Davis, and D. Crouse. The authors gratefully acknowledge support from the Applied Research for the Advancement of S&T Priorities program of the Office of the Secretary of Defense.

Competing financial interests:

The authors declare no competing financial interests.

References

[1] J. W. Lu, E. Chen, M. Kabir, M. R. Stan, and S. A. Wolf, *Spintronics Technology: Past, Present and Future*, Int. Mater. Rev. **61**, 456 (2016).

[2] H. L. Wang, C. H. Du, Y. Pu, R. Adur, P. C. Hammel, and F. Y. Yang, *Scaling of Spin Hall Angle in 3d, 4d, and 5d Metals from $Y_3Fe_5O_{12}$/Metal Spin Pumping*, Phys. Rev. Lett. **112**, 197201 (2014).

[3] W. Skowroński, Ł. Karwacki, S. Ziętek, J. Kanak, S. Łazarski, K. Grochot, T. Stobiecki, P. Kuświk, F. Stobiecki, and J. Barnaś, *Determination of Spin Hall Angle in Heavy-Metal/Co-Fe-B-Based Heterostructures with Interfacial Spin-Orbit Fields*, Phys. Rev. Appl. **11**, 024039 (2019).

[4] X. Tao, Q. Liu, B. Miao, R. Yu, Z. Feng, L. Sun, B. You, J. Du, K. Chen, S. Zhang, L. Zhang, Z. Yuan, D. Wu, and H. Ding, *Self-Consistent Determination of Spin Hall Angle and Spin Diffusion Length in Pt and Pd: The Role of the Interface Spin Loss*, Sci. Adv. **4**, eaat1670 (2018).

[5] M. Z. Hasan and C. L. Kane, *Colloquium: Topological Insulators*, Rev. Mod. Phys. **82**, 3045 (2010).

[6] A. Bansil, H. Lin, and T. Das, *Colloquium: Topological Band Theory*, Rev. Mod. Phys. **88**, 021004 (2016).

[7] Y. Fan, P. Upadhyaya, X. Kou, M. Lang, S. Takei, Z. Wang, J. Tang, L. He, L.-T. Chang, M. Montazeri, G. Yu, W. Jiang, T. Nie, R. N. Schwartz, Y. Tserkovnyak, and K. L. Wang, *Magnetization Switching through Giant Spin–Orbit Torque in a Magnetically Doped Topological Insulator Heterostructure*, Nat. Mater. **13**, 699 (2014).

[8] G. M. Stephen, I. Naumov, S. Tyagi, O. A. Vail, J. E. DeMell, M. Dreyer, R. E. Butera, A. T. Hanbicki, P. J. Taylor, I. Mayergoyz, P. Dev, and A. L. Friedman, *Effect of Sn Doping on Surface States of Bi_2Se_3 Thin Films*, J. Phys. Chem. C **124**, 27082 (2020).

[9] V. M. Edelstein, *Spin Polarization of Conduction Electrons Induced by Electric Current in Two-Dimensional Asymmetric Electron Systems*, Solid State Commun. **73**, 233 (1990).

[10] M. I. Dyakonov and V. I. Perel, *Current-Induced Spin Orientation of Electrons in Semiconductors*, Phys. Lett. A **35**, 459 (1971).

[11] C. H. Li, O. M. J. Van't Erve, J. T. Robinson, Y. Liu, L. Li, and B. T. Jonker, *Electrical Detection of Charge-Current-Induced Spin Polarization Due to Spin-Momentum Locking in Bi_2Se_3*, Nat. Nanotechnol. **9**, 218 (2014).

[12] T. S. Ghiasi, A. A. Kaverzin, P. J. Blah, and B. J. van Wees, *Charge-to-Spin Conversion by the Rashba–Edelstein Effect in Two-Dimensional van Der Waals Heterostructures up to Room Temperature*, Nano Lett. **19**, 5959 (2019).

[13] W. Luo, W. Y. Deng, H. Geng, M. N. Chen, R. Shen, L. Sheng, and D. Y. Xing, *Perfect Inverse Spin Hall Effect and Inverse Edelstein Effect Due to Helical Spin-Momentum Locking in Topological Surface States*, Phys. Rev. B **93**, 115118 (2016).

[14] A. Manchon, H. C. Koo, J. Nitta, S. M. Frolov, and R. A. Duine, *New Perspectives for Rashba Spin–Orbit Coupling*, Nat. Mater. **14**, 871 (2015).

[15] Y. K. Kato, R. C. Myers, A. C. Gossard, and D. D. Awschalom, *Observation of the Spin Hall Effect in Semiconductors*, Science **306**, 1910 (2004).

[16] J. Zhang, J. P. Velev, X. Dang, and E. Y. Tsymbal, *Band Structure and Spin Texture of Bi2Se3 3d Ferromagnetic Metal Interface*, Phys. Rev. B **94**, 014435 (2016).

[17] J. M. Marmolejo-Tejada, K. Dolui, P. Lazić, P.-H. Chang, S. Smidstrup, D. Stradi, K. Stokbro, and B. K. Nikolić, *Proximity Band Structure and Spin Textures on Both Sides of Topological-Insulator/Ferromagnetic-Metal Interface and Their Charge Transport Probes*, Nano Lett. **17**, 5626 (2017).

[18] Y.-T. Hsu, K. Park, and E.-A. Kim, *Hybridization-Induced Interface States in a Topological-Insulator–Ferromagnetic-Metal Heterostructure*, Phys. Rev. B **96**, 235433 (2017).

[19] D. A. Abanin, A. V. Shytov, L. S. Levitov, and B. I. Halperin, *Nonlocal Charge Transport Mediated by Spin Diffusion in the Spin Hall Effect Regime*, Phys. Rev. B **79**, 035304 (2009).

[20] G. M. Stephen, A. T. Hanbicki, T. Schumann, J. T. Robinson, M. Goyal, S. Stemmer, and A. L. Friedman, *Room-Temperature Spin Transport in Cd_3As_2*, ACS Nano **15**, 5459

(2021).

[21] G. M. Stephen, O. A. Vail, J. Lu, W. A. Beck, P. J. Taylor, and A. L. Friedman, *Weak Antilocalization and Anisotropic Magnetoresistance as a Probe of Surface States in Topological $Bi_2Te_xSe_{3-x}$ Thin Films*, Sci. Rep. **10**, 4845 (2020).

[22] C. Chen, D. Tian, H. Zhou, D. Hou, and X. Jin, *Generation and Detection of Pure Spin Current in an H-Shaped Structure of a Single Metal*, Phys. Rev. Lett. **122**, 016804 (2019).

[23] A. Hoffmann, *Spin Hall Effects in Metals*, IEEE Trans. Magn. **49**, 5172 (2013).

[24] X. Lou, C. Adelmann, S. A. Crooker, E. S. Garlid, J. Zhang, K. S. M. Reddy, S. D. Flexner, C. J. Palmstrøm, and P. A. Crowell, *Electrical Detection of Spin Transport in Lateral Ferromagnet–Semiconductor Devices*, Nat. Phys. **3**, 197 (2007).

[25] J. Tian, I. Miotkowski, S. Hong, and Y. P. Chen, *Electrical Injection and Detection of Spin-Polarized Currents in Topological Insulator Bi_2Te_2Se*, Sci. Rep. **5**, 14293 (2015).

[26] J. Tian, S. Hong, I. Miotkowski, S. Datta, and Y. P. Chen, *Observation of Current-Induced, Long-Lived Persistent Spin Polarization in a Topological Insulator: A Rechargeable Spin Battery*, Sci. Adv. **3**, e1602531 (2017).

[27] S. M. Farzaneh and S. Rakheja, *Intrinsic Spin Hall Effect in Topological Insulators: A First-Principles Study*, Phys. Rev. Mater. **4**, 114202 (2020).

[28] J. Han, A. Richardella, S. A. Siddiqui, J. Finley, N. Samarth, and L. Liu, *Room-Temperature Spin-Orbit Torque Switching Induced by a Topological Insulator*, Phys. Rev. Lett. **119**, 077702 (2017).

[29] K. Kondou, R. Yoshimi, A. Tsukazaki, Y. Fukuma, J. Matsuno, K. S. Takahashi, M. Kawasaki, Y. Tokura, and Y. Otani, *Fermi-Level-Dependent Charge-to-Spin Current Conversion by Dirac Surface States of Topological Insulators*, Nat. Phys. **12**, 1027 (2016).

[30] A. R. Mellnik, J. S. Lee, A. Richardella, J. L. Grab, P. J. Mintun, M. H. Fischer, A. Vaezi, A. Manchon, E.-A. Kim, N. Samarth, and D. C. Ralph, *Spin-Transfer Torque Generated by a Topological Insulator*, Nature **511**, 449 (2014).

[31] Y. Ji, A. Hoffmann, J. S. Jiang, J. E. Pearson, and S. D. Bader, *Non-Local Spin Injection in Lateral Spin Valves*, J. Phys. D. Appl. Phys. **40**, 1280 (2007).

[32] J. Tang, L.-T. Chang, X. Kou, K. Murata, E. S. Choi, M. Lang, Y. Fan, Y. Jiang, M. Montazeri, W. Jiang, Y. Wang, L. He, and K. L. Wang, *Electrical Detection of Spin-Polarized Surface States Conduction in $(Bi_{0.53}Sb_{0.47})_2Te_3$ Topological Insulator*, Nano

Lett. **14**, 5423 (2014).

[33] A. Narayanan, M. D. Watson, S. F. Blake, N. Bruyant, L. Drigo, Y. L. Chen, D. Prabhakaran, B. Yan, C. Felser, T. Kong, P. C. Canfield, and A. I. Coldea, *Linear Magnetoresistance Caused by Mobility Fluctuations in N-Doped* Cd_3As_2, Phys. Rev. Lett. **114**, 117201 (2015).

[34] R. Sehr and L. R. Testardi, *The Optical Properties of P-Type* Bi_2Te_3*-*Sb_2Te_3 *Alloys between 2–15 Microns*, J. Phys. Chem. Solids **23**, 1219 (1962).

[35] Z. Wang, T. Lin, P. Wei, X. Liu, R. Dumas, K. Liu, and J. Shi, *Tuning Carrier Type and Density in* Bi_2Se_3 *by Ca-Doping*, Appl. Phys. Lett. **97**, 042112 (2010).

[36] H. Köhler and E. Wöchner, *The G-Factor of the Conduction Electrons in* Bi_2Se_3, Phys. Status Solidi **67**, 665 (1975).

[37] H. Nakayama, K. Ando, K. Harii, T. Yoshino, R. Takahashi, Y. Kajiwara, K. Uchida, Y. Fujikawa, and E. Saitoh, *Geometry Dependence on Inverse Spin Hall Effect Induced by Spin Pumping in* $Ni_{81}Fe_{19}$*/Pt Films*, Phys. Rev. B **85**, 144408 (2012).

[38] D. Pesin and A. H. MacDonald, *Spintronics and Pseudospintronics in Graphene and Topological Insulators*, Nat. Mater. **11**, 409 (2012).

[39] See Supplemental Material at [URL will be inserted by publisher] for further information on the background subtraction and fitting.